Max Biegler, Angelina Marko, Benjamin Graf, Michael Rethmeier

# Finite element analysis of in-situ distortion and bulging for an arbitrarily curved additive manufacturing directed energy deposition geometry



Biegler, M.; Marko, A.; Graf, B.; Rethmeier, M. (2018). Finite element analysis of in-situ distortion and bulging for an arbitrarily curved additive manufacturing directed energy deposition geometry. Additive Manufacturing, 24, 264–272. https://doi.org/10.1016/j.addma.2018.10.006

# Finite element analysis of in-situ distortion and bulging for an arbitrarily curved directed energy deposition geometry

*Additive Manufacturing*

M. Biegler[1, #], A. Marko[1], B. Graf[1], M. Rethmeier[1,2,3]

[1]Fraunhofer Institute of Production Systems and Design Engineering (IPK),

Pascalstrasse 8-9 10587 Berlin

[2] Federal Institute of Materials Research and Testing (BAM)

Unter den Eichen 87. 12205 Berlin Germany

[3] Institute of Machine Tools and Factory Management, Technical University Berlin

Pascalstrasse 8-9 10587 Berlin

[#] Corresponding author:

Max Biegler

e-mail: max.biegler@ipk.fraunhofer.de, phone: +49 30 39006 404

## Abstract

With the recent rise in the demand for additive manufacturing (AM), the need for reliable simulation tools to support experimental efforts grows steadily. Computational welding mechanics approaches can simulate the AM processes but are generally not validated for AM-specific effects originating from multiple heating and cooling cycles. To increase confidence in the outcomes and to use numerical simulation reliably, the result quality needs to be validated against experiments for in-situ and post-process cases. In this article, a validation is demonstrated for a structural thermomechanical simulation model on an arbitrarily curved Directed Energy Deposition (DED) part: at first, the validity of the heat input is ensured and subsequently, the model's predictive quality for in-situ deformation and the bulging behaviour is investigated. For the in-situ deformations, 3D-Digital Image Correlation measurements are conducted that quantify periodic expansion and shrinkage as they occur. The results show a strong dependency of the local stiffness of the surrounding geometry. The numerical simulation model is set up in accordance with the experiment and can reproduce the measured 3-dimensional in-situ displacements. Furthermore, the deformations due to removal from the substrate are quantified via 3D-scanning, exhibiting considerable distortions due to stress relaxation. Finally, the prediction of the deformed shape is discussed in regards to bulging simulation: to improve the accuracy of the calculated final shape, a novel extension of the model relying on the modified stiffness of inactive upper layers is proposed and the experimentally observed bulging could be reproduced in the finite element model.



**Keywords:** DED; Welding simulation; Additive Manufacturing; Dimensional accuracy; Digital Image Correlation

# 1. Introduction

Recently, additive manufacturing (AM) techniques have been adopted into industrial practice, as they allow the build-up of complex geometries with near net-shape and large freedom-of-design compared to established machining approaches. In Directed Energy Deposition (DED), 3-dimensional components are built by locally welding multiple layers of additional material from powder or wire feedstocks onto a substrate [1]. During welding, the substrate and the already-deposited material are re-heated periodically with each new layer creating complex interlocking effects such as inhomogeneous thermal strains, local melting and shrinking, annealing and phase transformations. When building DED parts such as turbine housings [2] or excavator arms [3], the whole process is set up experimentally and has to be iterated a number of times to identify suitable parameters regarding – for instance – power and material feed, path planning strategies and cooling times between layers. These setups consume valuable personnel and machine times, before an adequate result quality is achieved and the part can go into production. With numerical simulations the experimental effort for parameter search, build-planning and shape optimization in DED can be reduced by conducting virtual tests before experimental trials and narrowing down the parameters. To introduce simulation tools for industrial applications, challenges regarding long calculation times, the availability of AM-specific material data and the difficulty of generating reference measurements for validation of the models need to be overcome.

As reference for the validity of a numerical simulation model, the temperature field and development of strains and distortions during build-up and in the finished part are usually compared to experimental data. In literature, a number of validation cases have been published for industrial-size components in joining, e.g. for a car door [4] or a circumferential pipe weld [5], comparing both in-situ displacements, residual distortions and stresses with the simulation results. Because the samples are built in the process, the acquisition of in-situ data for experimental validation is more demanding in additive manufacturing than in joining – i.e. the sample cannot be prepared before welding. To work around this difficulty, several industrial-scale AM-parts were simulated and compared to measurements taken on the finished part: Papadakis et al. [2] conducted a structural numerical welding simulation for a large aero-engine housing build and compared the results to experimental 3D-scans on the finished component. Marimuthu

et al. [6] calculated the displacement of the substrate in an aero-engine build and compared it to ex-situ coordinate machine measurements (CMM). Afazov and co-workers [7] used optical 3D-metrology to compare experimental and simulated distortions in selective laser melting (SLM) and developed a compensated geometry with reduced distortions. Ghasri-Khouzani et al. [8] measured distortion via CMM and residual stresses via neutron diffraction for SLM cylinders with varying thicknesses. Wang [9] and Mukherjee [10] simulated residual stresses for Inconel 625 and Ti-6AL-4V DED walls and used post-process measurements for validation. San Sebastian et al. [11] measured the deformation of a SLM cantilever after electric-discharge machining (EDM) cutting of the support structures with a dial gauge. In these publications, the measurements were conducted on the resulting shape and compared to the final outcome of the simulation. Because in-situ measurements are not available, the origin of deviations between experiment and simulation cannot be traced: The particular strength of numerical simulations – i.e. to illustrate and quantify transient effects as they occur – cannot be validated and hence cannot be utilized with confidence.

In-situ measurements in DED are also available, but they usually employ a 1-dimensional laser distance sensor or tactile displacement sensor on the underside of a substrate with a large distance to the newly-built part: Heigel et al. [12] compared the in-situ displacements at the free end of a cantilever substrate during laser-cladding, Denlinger et al. [13] used a similar setup to evaluate electron beam direct manufacturing in experiments and simulations, specifically to compare different simulation cases regarding stress-relaxation modelling and evaluated the influence of inter-layer pause times on distortions [14]. Lundbäck et al. [15] measured shape deviations with several tactile sensors in contact with the substrate to validate their simulations. While these approaches generated in-situ measurements to compare with transient simulation results, they only quantified the combined forces acting on the substrate and did not allow the observation of specific effects directly on the component.

In a recent publication by Biegler et al. [16], a new measurement method was established to determine in-situ distortions directly on a DED wall sample during build-up. 3D-Digital Image Correlation (DIC) was utilized, extending previous works by Bakir et al. [17] for in-situ crack observation and by Agarwal et al. [18] for in-situ strain investigation during laser welding onto additive manufacturing DED. During

deposition, the DIC system takes pictures of a stochastic speckle pattern on the sample and tracks changes in the pattern resulting from straining and distortion of the underlying sample from two angles [19]. The method has recently found use in AM by Barlett et al. [20] to investigate in-situ stresses in SLM, by Wu et al. [21] to validate the distortion simulation of electric discharge machining substrate removal and  and by Xie et al. [22] to investigate in-situ strains in DED. In the previous study [16], the experimental results were compared to a structural finite-element simulation and qualitative as well as quantitative agreement of the transient distortions was reported for a wall-build but no data for complex, curved cases relevant to industrial practice were shown.

In this work, the method established in the prior publication is extended from a simple wall onto an arbitrarily curved, thin-walled DED component. The formation of displacements in the component are measured from two sides using in-situ DIC and subsequently compared to the elasto-plastic FE-model. Consistent with recent studies employing 3D-optical scanning, the sample is removed from the substrate and the distortions due to stress relaxation as well as the final simulated and actual part shapes are discussed. As described in literature [2, 23], structural simulation models tend to estimate bending of the whole geometry instead of bulging in DED. To address the bulging modelling an addition to the structural simulation approach is introduced: The Young's Modulus in the not-yet activated upper layers is artificially increased to inhibit bending and keep the model upright for bulging prediction. The results for the approach are shown and its viability is discussed.

## 2. Methods

### *2.1 Experimental procedure*

A thin-walled, curved DED geometry was manufactured from EN 1.4404 (AISI 316L) stainless steel powder (particle size distribution 45 µm – 106 µm) onto a 100 mm x 100 mm x 6 mm (length x width x height) substrate with the setup described in detail in [16]. The sample geometry was the curved outline of a turbine blade with two gently curved sides bound together by a sharp bend on one side and not connected on the other side (see Figure 1 a-b). It was abstracted from the cross section of a turbine blade geometry and chosen because of its varying curvature and high-stiffness at the tip and low stiffness at the free ends. During the build, a coaxial powder nozzle stacked single tracks with 400 W laser power,

0.6 m/min forward speed, 0.6 mm spot diameter and 7.5 g/min of powder flow. 20 tracks were deposited with a bi-directional strategy and 30 s pause time between layers, resulting in a height of 12.4 mm and 1.2 mm wall-thickness. Subsequently, the process was stopped to coat the sample with the stochastic pattern for the DIC measurement. 10 additional layers were deposited on top, while measuring in-situ displacements with the commercial 3D-Digital Image Correlation system GOM Aramis 4m at 5 Hz image acquisition frequency and 1 ms exposure time (Figure 1c). As described by Bakir [17] in investigations of hot-cracking and Agarwal [18] for laser welding in-situ measurements, overexposure of the sensors due to the bright process light could be avoided by using narrow bandpass optical filters, transmitting only wavelengths in the range of 810 nm ± 22.5 nm. To generate enough background light for the optical measurement, a defocused, monochromatic laser illuminated the sample with 808 nm light. Both "long" sides (concave and convex side; see Figure 1) of the sample were measured in separate trials and each measurement was repeated in triplicate. In the post processing, a uniform coordinate system was defined and the data was smoothed with a temporal and spatial moving average filter for the two nearest neighbours.

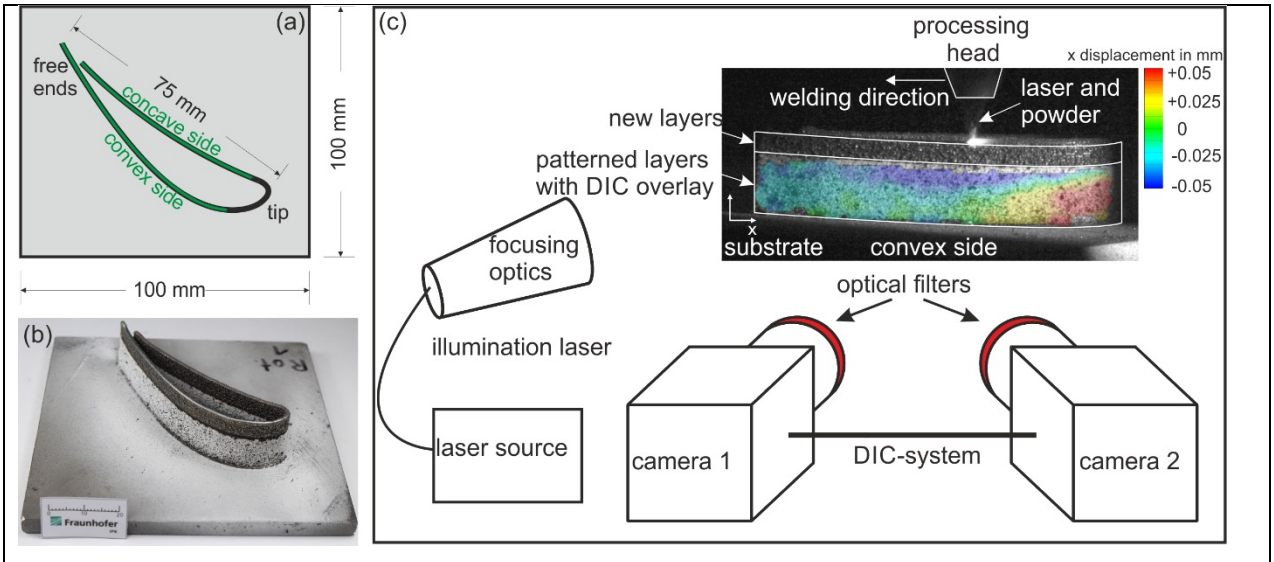


**Figure 1: Experimental setup.** (a): The geometry is shown from a top-down perspective. It is modelled after the outline of a turbine blade; The green surfaces labelled "concave-" and "convex side" were measured using DIC. (b): Photograph of the geometry after build-up. The DIC pattern is clearly visible on the lower 20 layers. (c): Experimental setup and in-situ DIC image with overlay for x-displacement during build-up. Image (c) altered from [16]

After the DIC measurements, three samples were 3D-scanned with a structured light 3D-scanner "GOM ATOS Triple Scan" using a 100 mm x 75 mm x 70 mm measuring volume with 30.6 µm measuring point distance and a maximum accuracy of 3 µm. Subsequently, the samples were removed from the substrate with electric discharge machining (EDM) and a second 3D-scan was conducted to quantify the distortions due to build-plate removal.

Finally, the distortions on the sides of the samples were measured at three characteristic lines using confocal microscopy (ALICONA InfiniteFocus) by stitching multiple confocal scans from the bottom of the part up to the top together with 5x magnification, 23.5 mm working distance and a height step of 5 µm. The gathered surface scans were averaged over 0.5 mm width to reduce the influence of adherent powder particles.

observation

### *2.2 Structural simulation procedure*

The transient elasto-plastic finite-element (FE) simulation was conducted in the commercial software simufact.welding 7.1 with the model described in [16]: in short, the model was meshed a priori and the to-be-deposited elements were deactivated via the quiet element method (or penalty method). The method includes all elements into the simulation from the start but reduces the material properties of the elements that are added due to material deposition with a penalty factor of $10^{-5}$ to the temperature dependent thermal and mechanical properties except for heat capacity. In order to prevent excessive deformation of the deactivated elements prior to activation as observed in [2], the Young's Modulus was set to a higher value of 10 GPa instead of applying the full penalty factor. After first trials, this formulation was identified as essential to model bulging: due to the increased stiffness of inactive elements the deformation in higher layers before activation can be reduced and a comparison is shown between 1 GPa and 10 GPa Young's modulus for the inactive zone. A cylindrical, phenomenological heat source heated and activated the model step by step, following the progress of the real build. As per the calibration done before, the heat source width was equal to the track width, the experimental energy input was scaled with an efficiency factor – describing the percentage of the laser coupled into the component – of 0.6 and the convective heat flow boundary was set to 35 W/m²K for all surfaces exposed

to air. The penalty factor was removed as the elements were heated above melting temperature (i.e. activated) by the moving heat source and subsequently cooled below solidus temperature, restoring the material properties listed in Table 1. Afterwards, the activated elements were considered to be solid material and their full contribution to the thermal and mechanical behaviour was included in all further increments.

To mimic the experiment, 20 layers were built and then a 300 s cooling break was implemented to reproduce the cooldown while applying the DIC pattern. Afterwards, 10 additional layers were deposited on top and the final cooling to room temperature was simulated. In each increment, the change in geometry, the heat generation and heat spread as well as the thermal strains, displacements and stresses were calculated according to the thermal and mechanical boundary conditions, the current model geometry and the material properties, as shown in Table 1 [24]. The model consisted of linear hexahedral elements and a mesh convergence study was conducted for three element sizes: The lowest element count with 1.2 mm edge length resulted in a single element over the thickness and a total of 5402 elements including the substrate, a single refinement lead to 0.6 mm edge length, 2 elements over the thickness and 27.032 hexahedrals, the third refinement step resulted in 0.3 mm edge length, 4 elements over the thickness and a total element count of 200.072 elements. The calculated maximum displacements changed 23.2 % between the unrefined and single-refinement model and between the single- and double-refinement models, the change was 1.6 %. With a weld length of ~155 mm per layer and a total of 4.65 m for the 30 layers in the whole part, the calculation time for the fully transient, coupled simulation was 8.8 hours for the unrefined, 25.3 hours on the single refinement and 148.2 h for the double-refinement model on a 16-core workstation. Taking into account the small change in accuracy and the greatly increased calculation time between the single- double-refinement models, the single-refinement model with 0.6 mm edge length was chosen for all investigations.

| Temperature in °C | 20 | 100 | 200 | 300 | 400 | 500 | 600 | 700 | 800 | 900 | 1000 | 1100 | 1200 | 1300 | 1400 | 1500 |
|---|---|---|---|---|---|---|---|---|---|---|---|---|---|---|---|---|
| Young's Modulus in GPa | 192 | 186 | 178 | 170 | 161 | 153 | 145 | 137 | 110 | 63 | 37 | 16 | 11 | 8 | 8 | 8 |
| Thermal Conductivity in W/mK | 14.0 | 15.1 | 16.4 | 17.8 | 19.1 | 20.5 | 21.8 | 23.2 | 24.5 | 25.9 | 27.2 | 28.6 | 29.9 | 31.3 | 32.6 | 34.0 |
| Specific Heat Capacity in J/kgK | 450 | 490 | 522 | 545 | 555 | 566 | 583 | 600 | 614 | 629 | 643 | 657 | 671 | 686 | 700 | 715 |
| Thermal Expansion Coefficient in $10^{-5}$ | 1.4 | 1.5 | 1.6 | 1.7 | 1.7 | 1.8 | 1.8 | 1.8 | 1.9 | 1.9 | 1.9 | 1.9 | 2.0 | 1.8 | 1.8 | 0 |
| Yield stress in MPa | 275 | 238 | 198 | 172 | 157 | 151 | 145 | 136 | 127 | 115 | 78 | 38 | 24 | 20 | 16 | 9 |

Table 1: Material properties of 316L for welding simulation [24]. In addition, 256.4 J/g was used for the enthalpy of melting, 8000 kg/m³ for the density and 0.3 for the Poisson's ratio.

After the build-up, an additional simulation step was added for the stress relaxation and deformation due to EDM removal of the part from the substrate. Following the machining direction, the lowest layer of elements (0.3 mm thickness) connecting the component to the substrate was removed from the simulation via an element death formulation. With the element death formulation, desired elements can be deleted from an ongoing simulation: The element itself is removed with its result values and the connectivity and stiffness matrices are adjusted accordingly. All surrounding elements keep their result values but a new mechanical equilibrium needs to be calculated in the next increment to account for the changed geometry in the part. As the removal progressed, residual stresses relaxed into part distortions according to the reduced clamping due to element deletion. In the final step, the whole substrate was removed and a new mechanical equilibrium was calculated according to the changed boundary. During the relaxation calculation, the newly-built component was fixed only at a single point to simulate an unconstrained transformation of stresses into displacements. A similar formulation was used by Papadakis [2] to evaluate the final shape of their component and compare it to experimental 3D-scans and by Salonitis et al. [25] to simulate stress relaxation due to high speed machining of a DED geometry. To evaluate the final shape of the deposited geometry for comparisons with the confocal scans, the out-of-plane bending at the corresponding locations was extracted from the model after all calculation steps.

### *2.3 Thermal calibration*

To ensure that the thermal calibration done only for a single track on the substrate in [16] remained valid for higher layers in large samples, the temperatures were measured in-situ on a DED wall. Two K-type thermocouples were micro-welded on the side of a wall sample and one on the substrate after 20 layers of deposition before continuing the build for 10 additional layers and measuring the temperatures with 300 Hz. The experimental measurements were reproduced in a thermal simulation with the same parameters used for the complex turbine-blade build and the temperature at the thermocouples was compared with the simulations. This thorough heat input and thermal boundary calibration is crucial, as errors in the thermal modelling propagate into the mechanical simulation, reducing the result quality. If possible, the thermal calibration should be carried out over several layers so that slight deviations between experiment and calculation can add up and become apparent [26].

## 3. Results and Discussion

### *3.1 Temperature input validation*

The results for the temperature calibration are depicted in Figure 2, showing a very good agreement between the measured and simulated temperature development for 10 added layers. Both the heat input – visible in the peaks – as well as thermal conduction and thermal boundaries – visible in the delays between the thermocouples and the cooling rates respectively – match well and no significant adding up of errors in the heat input is observed over more than 500 s process time. No changes from the calibrated heat input and boundaries done for a single track on the substrate [16] was necessary and the heat input is considered to be valid for the following mechanical calculation.

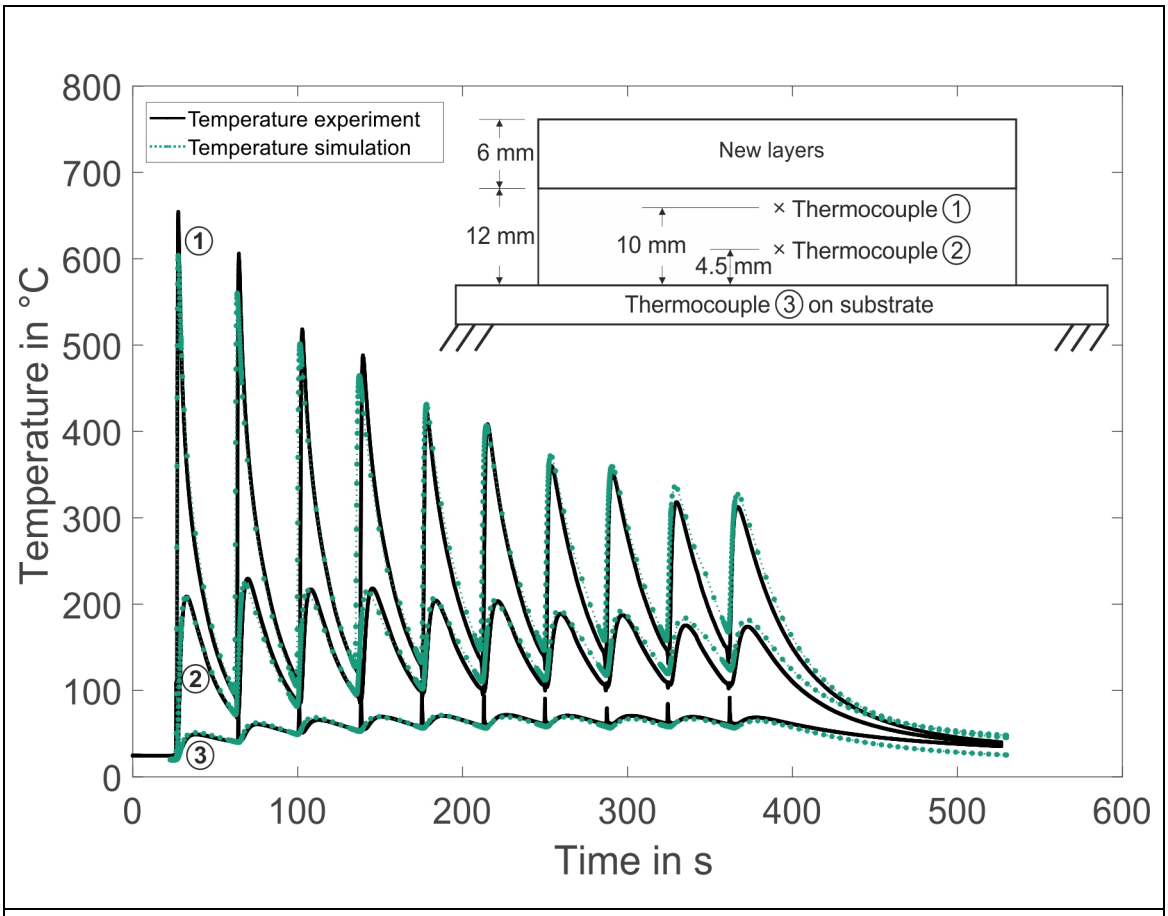


**Figure 2: Comparison of temperatures between experiment and simulations for higher layers of a DED wall.** Three thermocouples were fixed onto the wall after 20 layers to validate the FE heat input originally generated in a single-track experiment. Both the peaks and the cooling times match well for additional 10 layers of build-up without further adjustment.

The finding that the process energy absorption, i.e. the fraction of the laser power coupling into the component, remains constant for higher layers in this setup is in contrast to an article for a process simulation model of DED by Alimardani et al. [27]. In the investigation, the energy absorption drops from about 40 % in the first deposited layer to about 22 % in higher layers due to the steep sides of the deposited track reflecting the beam rather than absorbing it. However, the beam diameter was 1.4 mm and the deposit width was at roughly the same size with 1.49 mm. During the process described here, the beam diameter was half the size as the deposit width, with 0.6 mm beam diameter and 1.2 mm deposit width. Therefore, it is likely that the geometry is mostly flat at the area of incidence of the laser beam and no significant deflections occur, leading to a constant energy absorption across the whole build process.

### *3.2 Simulated distortion results*

Figure 3a shows the results of the numerical simulation with the total distortion overlay for 30 layers after cooling to room temperature. The colour overlay quantifies the deviations of the geometry in all coordinate directions after build-up in comparison to the idealized CAD. Close to the substrate, the geometry remains mostly undeformed but distortions add up due to repeated thermal loading as new layers are added. The largest shape deviations are observed around the curvature in the convex and concave sides of the geometry, likely because the bent areas not only create in-plane strains but also out-of-plane strains, introducing tilt, bulging and warping into the surfaces. The free ends also deform significantly; only the tip of the part distorts barely due to the rigidity of the small curvature radius. For the distortion-components in x-, y- and z-directions (Figure 3 b-d), the general tendencies of the deformations are visible in a global coordinate. In x-direction, corresponding closest to tangent / in-plane distortions, the inward bending of the tip and the free-ends is observed. Together with the downward bending in z-direction, the formation of a u-shape similar to [16] is calculated – i.e. the ends and turning points bend inward and the long edges of the concave and convex sides bend downward. In y-direction, the concave and convex sides show bulging behaviour with the convex side bulging inward – towards the center of the geometry and the concave side bulging outwards. The final shape for out-of-plane bulging in y-direction will be discussed in the following sections.

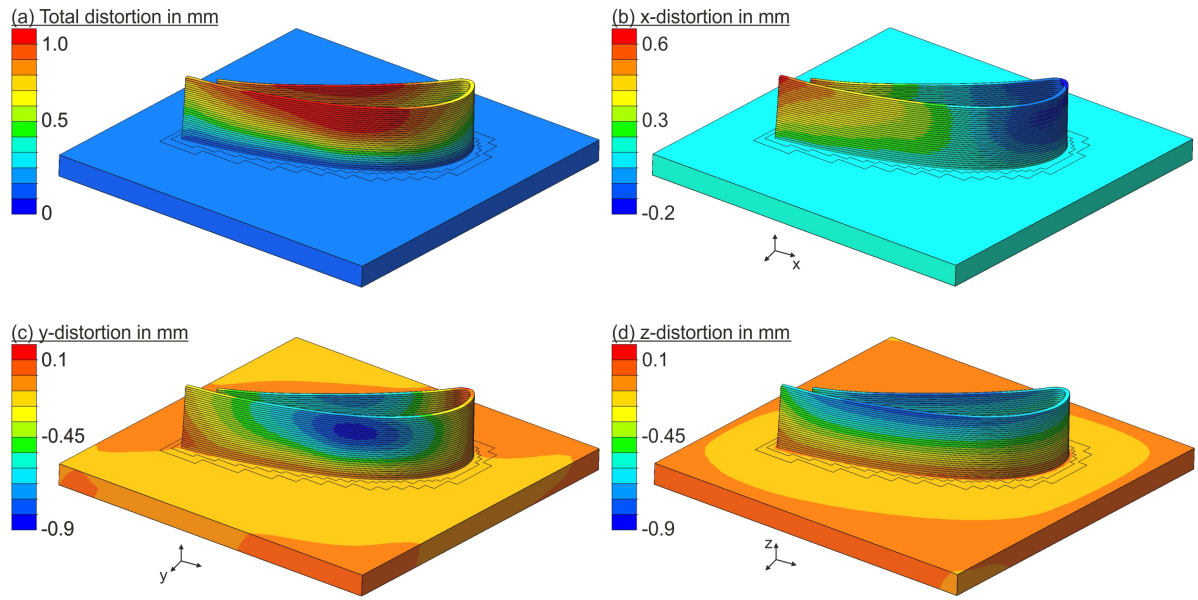


**Figure 3: Final distortion after 30 layer build-up simulation.** (a): The added up absolute values for displacements in x-, y- and z-directions are visible; The curved sides deform the most as – especially at higher layers – normal and tangential distortions occur. (b-d) show the displacements in the global coordinate system with the x-direction showing in-plane inward bending, the y-direction out of plane bulging at the concave and convex sides and the z-direction downward shrinking.

### *3.3 Comparison of simulated and measured in-situ displacements*

In order to draw comparisons between the simulation and the experiments, the transient displacements at a total of six discrete points, evenly spaced across the two DIC surfaces (Figure 4), are extracted. The points are located at 9 mm height from the substrate, where significant distortions occur and the DIC system could still measure reliably. As the DIC measurement sets the first frame after the application of the stochastic pattern as reference, the simulated displacements are set to zero after 20 layers and synchronized with the experiments. Both experimental and simulated displacements are transformed into “tangent” and “normal” displacements via a coordinate transformation with respect to the local curvature at each point. The normal direction is orthogonal to the local curvature, the height direction points upwards and the tangent direction is oriented according to a right-hand coordinate system, pointing in circumferential / in-plane direction. The transformation allows the consideration of the distortion evolution regardless of the local curvature and is identified to be a necessary step in the evaluation of a curved part. Similar coordinate system notations were already utilized by Papadakis [2]

and Ghasri-Khouzani [8] for cylinder and disc builds, respectively. The results are shown in Figure 4 for tangent, normal and height displacements with experimental mean and standard deviations from three independent trials and the simulation results superimposed at all six investigated points. For all investigated points, the AM specific saw-tooth behaviour due to the repeated heating and cooling cycles is clearly visible. The tangential and normal displacements show a strong dependency on the local curvature and stiffness: Close to the rigid tip, displacements are small, whereas they reach high values in the low-stiffness, curving areas. In general, the simulation slightly underestimates the experiments but matches the qualitative behaviour very well:

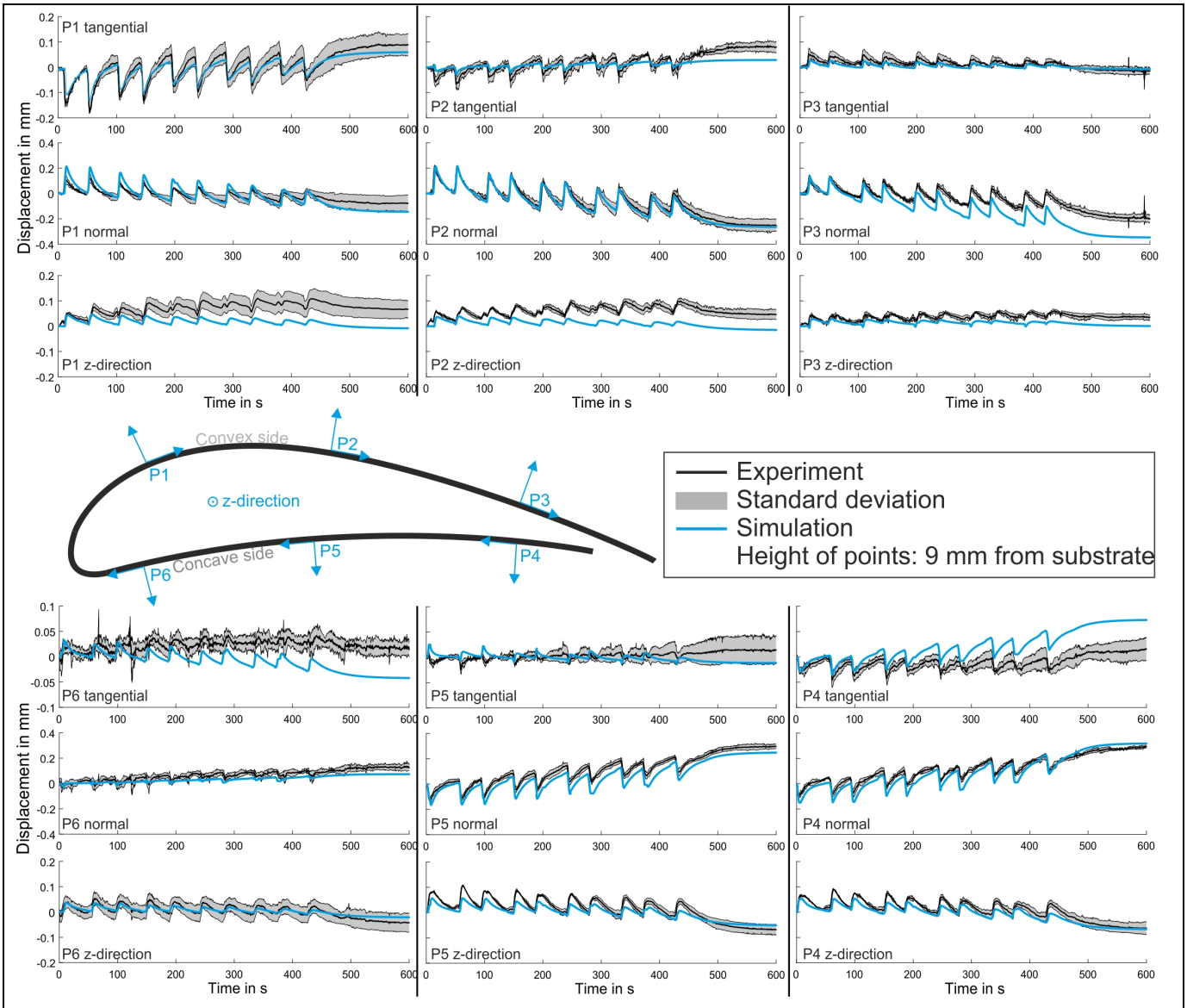


**Figure 4: Comparison of in-situ distortions.** The in-situ distortions are compared at six discrete points along the test geometry between experiment (black lines with grey standard deviation from three independent trials) and simulation (blue lines). The points are located at 9 mm height from the substrate and transformed into tangential-, normal- and z-direction according to the local curvature.

For the tangential direction, the transient displacements are comparatively small across the whole part. The values are lying between -0.1 mm and 0.1 mm at the edges, whereas the middle of the flat geometry is almost not moving at P5. The largest tangential displacements occur at P1 together with the greatest experimental scatter: due to the small curvature radius at the tip, the heat input is very concentrated as demonstrated by Zhang [23]. P1 is located directly next to the large gradients and has lower stiffness than the tip so that it is displaced significantly during the process. The high amount of scatter between the experiments is likely also due to the location of the point. With the single laser illumination source, the areas of large curvature were difficult to illuminate consistently especially between samples. All other points in tangential direction indicate a good fit between simulation and experiment with deviations at P4 and P6 as well as a high reproducibility between samples.

By far the largest displacements are measured and calculated in normal direction. On the convex side, the part expands outward (positive in normal direction) and shrinks inward upon cooling, leaving a significant distortion of up to -0.35 mm for P2 and P3. The deformation direction on the concave side is inverted, with the expansion pointing inward (negative in normal direction) and expansion pointing outward with distortion magnitudes of about 0.33 mm after cooling similar to the convex side. P1 and especially P6 exhibit smaller transient displacements due to their proximity to the rigid tip. Significant out-of-plane distortion remains after the process, hinting at bending or bulging and the final shape is discussed below together with the post-process measurements. For the z-direction, the sample expands upward and shrinks downward. The displacements are mostly small and generally slightly underestimated in the simulation. Due to the free expansion and shrinking in height-direction, little deformation remains after cooling.

With the presented in-situ measurement technique, the displacements occurring during the process can be quantified and compared to the simulation and reproducible results can be achieved especially for the gently-curving areas. The distortion measurement has to be started on a pre-built geometry and all distortions are referenced to the first image taken by the system before the process is continued: As the same repeated thermal loadings that lead to the distortions during the DIC measurements act on the lower layers during build-up, the zero-reference of the DIC system is on an already distorted geometry

and the layers deposited on top of the patterned area cannot be regarded with the technique. Hence, different methods are required to evaluate the final, distorted shape of the geometry. For experimental reference, two different methods relying on post process optical measurements (i.e. 3D-scanning and confocal microscopy) are utilized for removal from the substrate and the final part shape.

### *3.4 Distortions due to substrate removal*

Removal of newly-built parts using electric-discharge machining (EDM) is commonly used in additive manufacturing and leads to stresses relaxing into distortions [21]. In this work, the parts are separated from the substrate after the DIC measurements with optical 3D-scanning prior- and post-removal to quantify the changes. The EDM process is simulated by progressively removing the lowest row of elements in contact with the substrate after the DED simulation and calculating new mechanical equilibria according to the changed contact conditions. The substrate is deactivated from the model after all connecting elements have been deleted and the final distortions are quantified.

In Figure 5, the stress relief upon removal from the substrate is demonstrated after the build-up simulation. In (a), the von-Mises residual stresses after the build are depicted: they reach values of up to 450 MPa close to the substrate, falling to a minimum at about 75 % of the height and increasing to about 350 MPa at the top. A similar qualitative behaviour with peak values at the base plate and a minimum in the middle of the wall was observed in numerical simulations for wall builds of Inconel 625 by Wang et al. [9] and by Mukherjee et al. [10] for Ti-6Al-4V and Inconel 718. While these studies focused on straight walls and different materials, the general behaviour is comparable – especially for the almost-straight free edges of the turbine blade – indicating that the results in Figure 5a are consistent with the literature.

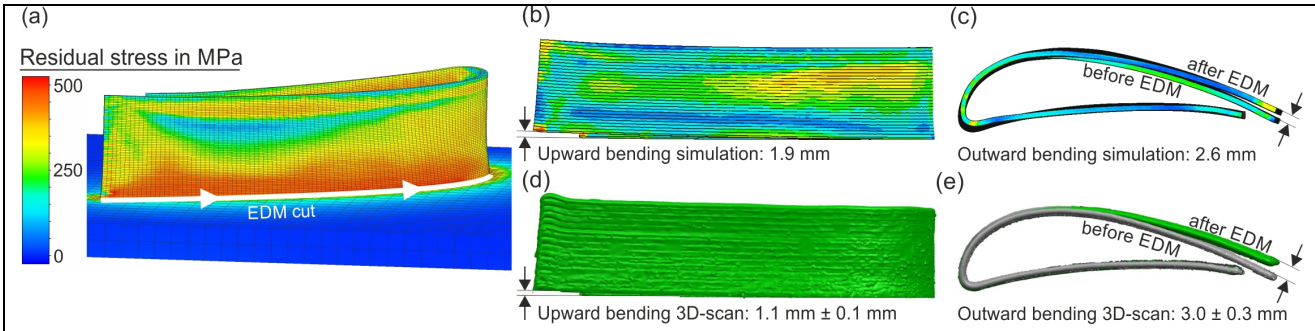


**Figure 5: Simulation of the substrate-removal via EDM.** In (a), the residual stress distribution after build-up is visible. As the part is separated (b), the residual stresses relax into distortions and far smaller stresses remain in the part. In (c), the shapes before and after removal from the substrate are superimposed. The biggest deformations occur at the free end of the convex side. In (d) and (e), the results of the 3D-scans (grey before removal, green after EDM) show agreement with the simulations in distortion direction and magnitude.

In Figure 5b, the deformation of the relaxed part is depicted for the convex side. Residual stresses are relieved especially at the area formerly connected to the substrate and an upward bending of 1.9 mm at the free end is calculated. In the top-down view (Figure 5c), an outward bending with a magnitude of 2.6 mm at the free end of the convex side is visible in the overlay between the before- and after-EDM contours; the concave side and the tip exhibit no discernible displacements. Reference measurements were conducted via 3D-structured-light-scanning for three independent trials and the results are depicted in Figure 5d and 5e: The shapes and directions of simulations and experiments match, in both the upward and outward bending of the convex side: With 1.9 mm estimated upward bending versus 1.1 mm ± 0.1 mm actual bending and 2.6 mm outward bending versus 3.0 mm ± 0.3 mm actual outward bending. Although the stress modelling is simplified with effects from multiple reheating creep and microstructure changes being neglected, the results are in good agreement with only slight quantitative deviations.

In comparison to other EDM removals shown in the literature for instance by Papadakis [2] for a DED geometry or by Wu et al. [21] for SLM, the deformations of the investigated geometry are large, because the sample has an open side that can deform freely: the tip forces the long sides apart like a spring due to the release of residual stresses. It is comparable to deformations described by San Sebastian et al. [11] for the free ends of a SLM cantilever after cutting of the support structure. In the cantilever, the ends are also unconstrained and can relax freely.

### *3.5 Bulging prediction*

To assess the final geometric accuracy of the experiment and compare it to the simulated shape after EDM, the sides are scanned using confocal microscopy. The scans are all done from the side formerly connected to the substrate to the top, averaging over 0.5 mm width to reduce scatter on the surface e.g. from adherent powder particles. Subsequently the data is zeroed at the point closest to the substrate and averaged over three independent trials. Three representative locations – on the convex side close to the tip and close to the free end as well as in the middle of the concave side – are chosen for Figure 6. The same coordinate convention as for the DIC measurements is kept with negative values denoting bending inward – i.e. away from the viewer – and positive values denoting outward bending. For clarity, the dashed grey line stands for the position at which the DED system deposits the material; the closer the measurements adhere to that line, the smaller the distortions.

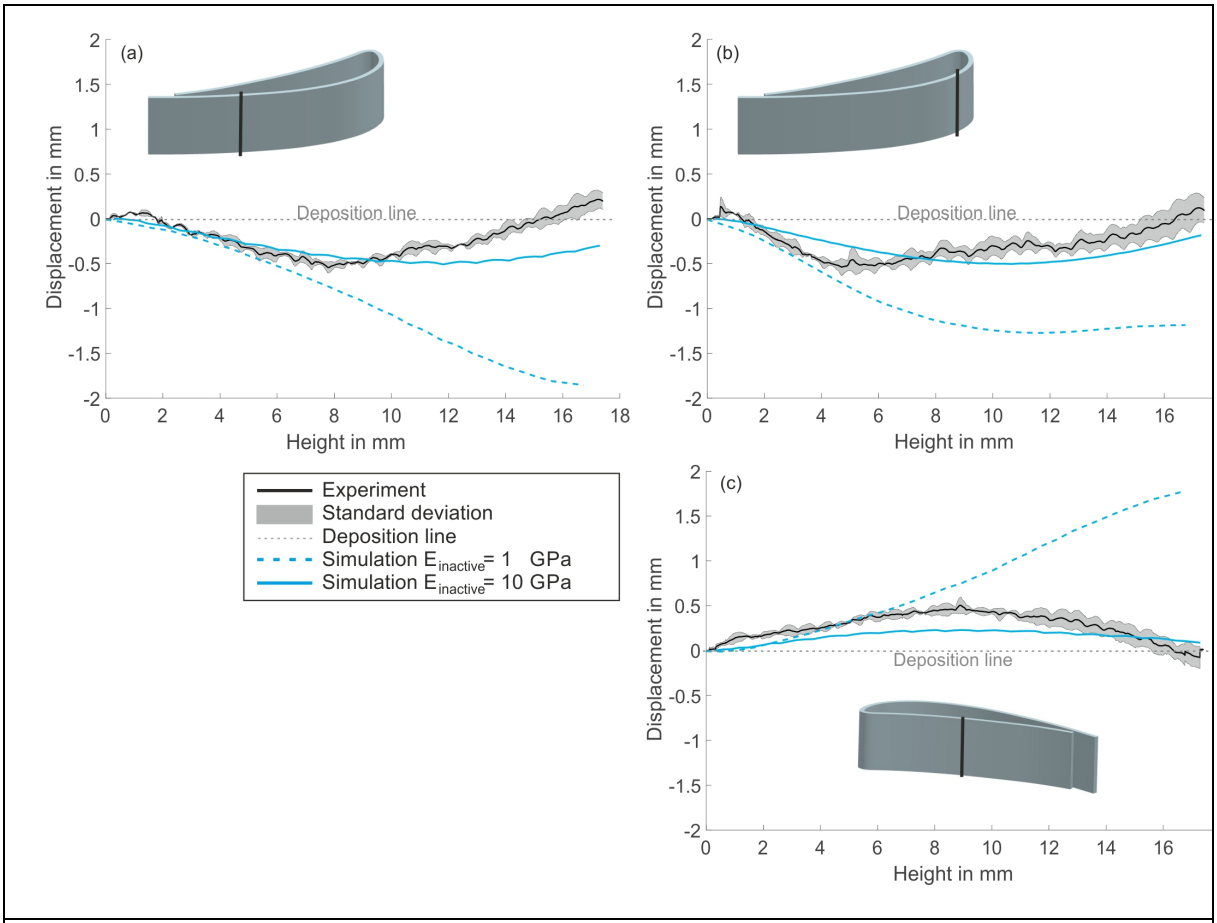


**Figure 6: Comparison of the final distortion profile measured with confocal microscopy at three lines.** In (a) and (b), the inward bulging is measured and in (c), the geometry bulges outwards. The difference between the two simulation cases with different Young's Moduli of inactive elements is well visible: the 1 GPa variant does not reproduce the bulging and the whole geometry tilts to the side for all three locations whereas the 10 GPa variant is stabilized by the higher stiffness and

reproduces comparable bulging. Experimental average and standard deviation from three independent trials.

The experimental results show inward bulging for the convex side and outward bulging for the concave side: this behaviour is consistent with the in-situ DIC results in Figure 4, where all points on the convex side exhibit negative normal bending and points 4 and 5 on the concave side deform in the outward direction. The bulging behaviour can be explained with the DED process: As additional layers are always deposited on the same line – merely with an added height-step – the most recently deposited layers are undeformed and in line with the machine code. Only the layers below deform due to the thermal gradients, exhibiting bulging in the direction of the curve's center points. Similar bulging of a cylindrical geometry was also observed by Salonitis [25] for their numerical studies and by Papadakis [2] for experimental and numerical investigations. In these studies, only closed cylinders were investigated that bulged inward – i.e. towards the center point; the outward bulging of the convex side shown here can be explained with the same mechanism but an inverted, outward-lying center point.

The simulated results are transformed into the same coordinate system and the calculated normal distortions are overlaid with the experimental results in Figure 6. The solid blue lines stand for the final simulation case that was shown in the DIC measurements. In general, the measured residual distortions are reproduced and the simulation results exhibit comparable bulging. Two variants are simulated with different Young's moduli of the inactive elements to discuss bulging modelling in AM: for the first variant, the Young's modulus of the upper layers is set to 1 GPa until they are reached by the heat source and activated (dashed blue line), in the second variant it is increased ten-fold to 10 GPa (solid blue line). The increase of the Young's modulus is a first possible solution to a problem in DED modelling of thin-walled geometries described in [2] and visualized in Figure 7: the simulation model is defined a priori with the elements for all layers being present from the beginning. With the penalty method, the "inactive" elements are assigned reduced mechanical and thermal properties but can still move as lower-lying elements are activated and deformed due to thermal gradients. As the low-stiffness inactive elements are displaced, they are no longer on the deposition line as defined CAD, when the heat source passes them to be activated.

The deposition location of the DED process does not change in x- or y-direction and corrects the

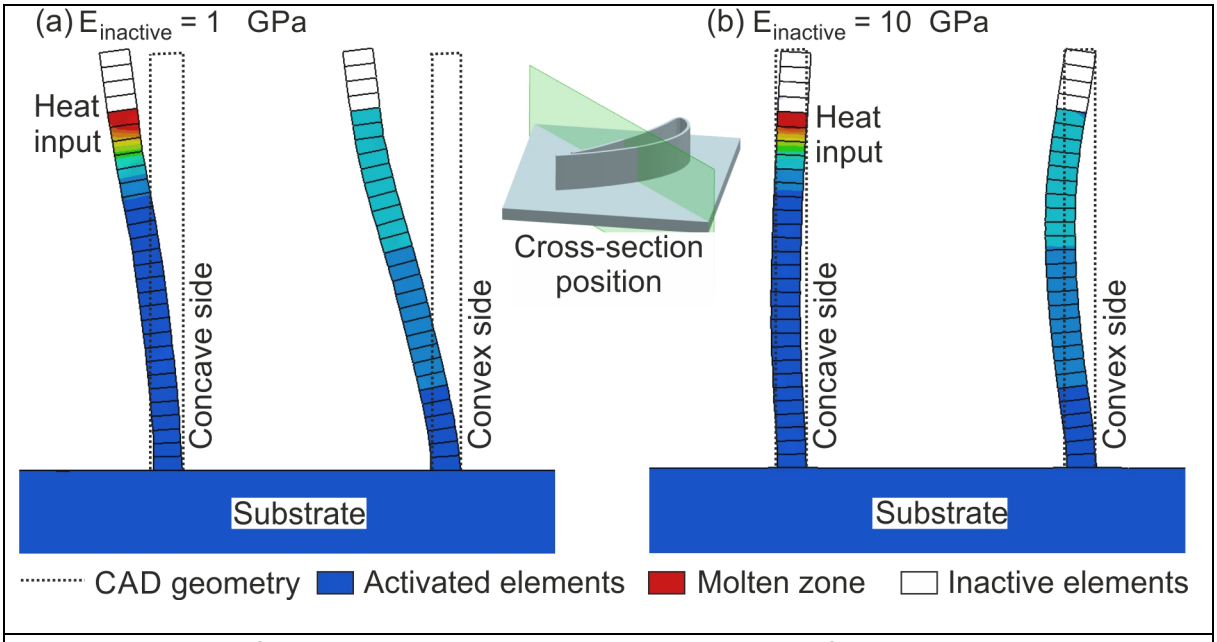


**Figure 7: Bending of the inactive layers causing mismatches in the final geometry.** Cross sections of the sample during welding of the 26th layer are shown with distortions magnified by a factor of 2 and individual element edges hidden for clarity. All layers above the momentary position of the heat source are inactive, the layers below active. In (a), the out-of-plane bending is excessive and the material activation takes place outside of the pre-designed machine path. In (b), the displacements are less pronounced because the inactive layers are assigned a higher stiffness of 10 GPa so that the model is kept upright and bulging is predicted instead of bending.

dimensional inaccuracies of lower layers somewhat by staying on the line specified in CAD. In the simulation, the inactive upper elements can be displaced with deformations in the lower layers and the heat source moves with them: the lower the stiffness of the inactive areas, the larger the pre-deformations. In Figure 7a ($E_{inactive} = 1$ GPa), bending is predicted and the inactive, uppermost layers are displaced significantly out of the CAD geometry. In Figure 7b ($E_{inactive} = 10$ GPa), the stiffened inactive elements hold the active elements in place so that the activation is taking place inside the CAD geometry. In the comparison between experiment and simulation in Figure 6, the bulging is approximated in the simulation models with increased stiffness in the inactive layers. This behaviour is especially apparent in Figure 6a and 6c, where the variant with the lower stiffness tilts to the outside instead of bulging. In general Figure 6, shows that the model with increased top-layer stiffness adheres much more closely to the experimental deformation shape: it exhibits the same bulging behaviour in negative direction for the convex and in positive direction for the concave side.

With these results, the increase of stiffness in the inactive layers is identified as a good measure to model bulging and ensure that the inactive elements are kept at the line defined in the machine code. However,

the stiffness used is geometry sensitive: Papadakis [2] calculated smaller deviations, although no additional stiffness was used, because the geometry was a closed cylinder and stiffer than the open-ended geometry here. On the other hand, the stiffness must not be chosen too large so that the deformations of the lower layers are impeded: with the value chosen here, no change in the DIC results are visible between the 1 GPa and the 10 GPa Young's modulus variants, proving that the inactive layers are not too stiff. Lastly, this formulation does not protect against excessive bending at the topmost layers, as the influence of the inactive layers lessens with the build progress. This explains the deviations in Figure 6 for the top of the samples: the experimental deformations are close to zero for the bottom – rigidly connected to the substrate before EDM – and the top – according to the deposition at the CAD coordinates. The simulated results do not return to zero for the last layers, because the geometry begins to bend for the highest layers with little support from the inactive layers. It would be possible to add more inactive layers to the model to keep it upright artificially but this is a purely stochastic approach that needs to be calibrated iteratively for geometries of differing stiffness. To solve this problem conclusively, an improved simulation model that keeps the current layer in place has to be developed in the future.

## 4. Conclusion

In this article, the validation of an elasto-plastic finite-element model for additive manufacturing directed energy deposition was shown on an arbitrarily-curved geometry. It expanded upon a prior work by investigating a more complex geometry with both in-situ and post-process distortion measurements.

- The heat input was validated for all layers by comparing thermal simulations for higher layers of a wall with experimental thermocouple measurements.
- 3D in-situ distortion measurements on a curved AM geometry were not yet reported in the literature and showed a strong dependency on local stiffness and curvature for the normal and tangent directions. In z-direction they were mostly geometry-independent.
- The simulation results were compared to the in-situ distortion measurements with good agreement. The inward bending in tangent and height directions as well as the bulging behaviour in normal direction was well-reproduced.

- The simulation formulation was extended with an element death formulation that allowed the estimation of EDM removal distortions. The simulated directions and magnitudes of deformations resulting from the stress relaxation were in good agreement with the experimental results.
- To evaluate the FE estimation of bulging, the model's final shape was compared to confocal scans of the sides. The unmodified simulation model estimated bending rather than bulging because of the displacement of inactive upper layers. A stochastic approach using a heightened stiffness in the inactive elements of upper layers to keep the model upright was proposed. This model extension allowed accurate prediction of the bulging behaviour on the sides in agreement with the measurements.

The results of the study add confidence to the use of structural finite-element simulation for prediction of DED part distortions in scientific and industrial cases: the presented approach can be used to predict distortions numerically and reduce experimental effort for industrial components and to study scientific questions regarding distortion, residual stress and temperature fields. As in-depth data for in-situ and post-process validation has been presented, the results can also be used as a reference case to test model additions and simplifications or to compare completely different simulation approaches for result accuracy and computational time.

**Acknowledgements**

The IGF-project 18737 N of the research association Forschungsvereinigung Stahlanwendung e.V. (FOSTA), Sohnstraße 65, 40237 Düsseldorf, was funded through the AiF within the program of the promotion of the industrial joint research (IGF) by the Federal Ministry for Economic Affairs and Energy based on a resolution of the Deutsche Bundestag.

## References

[1] W. E. Frazier, "Metal Additive Manufacturing: A Review," *J. of Materi Eng and Perform*, vol. 23, no. 6, pp. 1917–1928, 2014.

[2] L. Papadakis and C. Hauser, “Experimental and computational appraisal of the shape accuracy of a thin-walled virole aero-engine casing manufactured by means of laser metal deposition,” *Prod. Eng. Res. Devel.*, vol. 11, no. 4-5, pp. 389–399, 2017.
[3] S. Simunovic, A. Nycz, M. Noakes, C. Chin, V. Oancea, “Metal Big Area Additive Manufacturing: Process Modeling and Validation,” *NAFEMS World Congress 2017*, 2017.
[4] W. Perret, R. Thater, U. Alber, C. Schwenk, M. Rethmeier, “Approach to assess a fast welding simulation in an industrial environment — Application for an automotive welded part,” *Int.J Automot. Technol.*, vol. 12, no. 6, pp. 895–901, 2011.
[5] Z. Bézi and S. Szávai, “Repair Weld Simulation of Austenitic Steel Pipe,” *AMR*, vol. 1029, pp. 194–199, 2014.
[6] S. Marimuthu, D. Clark, J. Allen, Am Kamara, P. Mativenga, L. Li, R. Scudamore, “Finite element modelling of substrate thermal distortion in direct laser additive manufacture of an aero-engine component,” *Proceedings of the Institution of Mechanical Engineers, Part C: Journal of Mechanical Engineering Science*, vol. 227, no. 9, pp. 1987–1999, 2012.
[7] S. Afazov, W. A.D. Denmark, B. Lazaro Toralles, A. Holloway, A. Yaghi, “Distortion prediction and compensation in selective laser melting,” *Additive Manufacturing*, vol. 17, pp. 15–22, 2017.
[8] M. Ghasri-Khouzani, H. Peng, R. Rogge, R. Attardo, P. Ostiguy, J. Neidig, R. Billo, D. Hoelzle, M. R. Shankar, “Experimental measurement of residual stress and distortion in additively manufactured stainless steel components with various dimensions,” *Materials Science and Engineering: A*, vol. 707, pp. 689–700, 2017.
[9] Z. Wang, E. Denlinger, P. Michaleris, A. D. Stoica, D. Ma, A. M. Beese, “Residual stress mapping in Inconel 625 fabricated through additive manufacturing: Method for neutron diffraction measurements to validate thermomechanical model predictions,” *Materials & Design*, vol. 113, pp. 169–177, 2017.
[10] T. Mukherjee, W. Zhang, T. DebRoy, “An improved prediction of residual stresses and distortion in additive manufacturing,” *Computational Materials Science*, vol. 126, pp. 360–372, 2017.
[11] M. San Sebastian, I. Setien, A. M. Mancisidor, A. Echeverria, “SLM (Near)-Net-Shape Part Design Optimization Based on Numerical Prediction of Process Induced Distortions,” *TMS 2017 146th Annual Meeting & Exhibition Supplemental Proceedings*, 2017.
[12] J. C. Heigel, P. Michaleris, T. A. Palmer, “In situ monitoring and characterization of distortion during laser cladding of Inconel® 625,” *Journal of Materials Processing Technology*, vol. 220, pp. 135–145, 2015.
[13] E. R. Denlinger, J. C. Heigel, P. Michaleris, “Residual stress and distortion modeling of electron beam direct manufacturing Ti-6Al-4V,” *Proceedings of the Institution of Mechanical Engineers, Part B: Journal of Engineering Manufacture*, vol. 229, no. 10, pp. 1803–1813, 2014.
[14] E. R. Denlinger, J. C. Heigel, P. Michaleris, T. A. Palmer, “Effect of inter-layer dwell time on distortion and residual stress in additive manufacturing of titanium and nickel alloys,” *Journal of Materials Processing Technology*, vol. 215, pp. 123–131, 2015.
[15] A. Lundbäck and L.-E. Lindgren, “Modelling of metal deposition,” *Finite Elements in Analysis and Design*, vol. 47, no. 10, pp. 1169–1177, 2011.
[16] M. Biegler, B. Graf, M. Rethmeier, “In-situ distortions in LMD additive manufacturing walls can be measured with digital image correlation and predicted using numerical simulations,” *Additive Manufacturing*, vol. 20, pp. 101–110, 2018.
[17] N. Bakir, A. Gumenyuk, M. Rethmeier, “Investigation of solidification cracking susceptibility during laser beam welding using an in-situ observation technique,” *Science and Technology of Welding and Joining*, vol. 23, no. 3, pp. 234–240, 2017.

[18] G. Agarwal, H. Gao, M. Amirthalingam, M.J.M. Hermans, “In situ strain investigation during laser welding using digital image correlation and finite-element-based numerical simulation,” *Science and Technology of Welding and Joining*, vol. 57, no. 3, pp. 1–6, 2017.
[19] B. Pan, K. Qian, H. Xie, A. Asundi, “Two-dimensional digital image correlation for in-plane displacement and strain measurement: A review,” *Meas. Sci. Technol.*, vol. 20, no. 6, p. 62001, 2009.
[20] J. L. Bartlett, B. P. Croom, J. Burdick, D. Henkel, X. Li, “Revealing mechanisms of residual stress development in additive manufacturing via digital image correlation,” *Additive Manufacturing*, vol. 22, pp. 1–12, 2018.
[21] A. S. Wu, D. W. Brown, M. Kumar, G. F. Gallegos, W. E. King, “An Experimental Investigation into Additive Manufacturing-Induced Residual Stresses in 316L Stainless Steel,” *Metall and Mat Trans A*, vol. 45, no. 13, pp. 6260–6270, 2014.
[22] R. Xie, Y. Zhao, G. Chen, X. Lin, S. Zhang, S. Fan, Q. Shi, “The full-field strain distribution and the evolution behavior during additive manufacturing through in-situ observation,” *Materials & Design*, vol. 150, pp. 49–54, 2018.
[23] A. Zhang, B. Qi, B. Shi, D. Li, “Effect of curvature radius on the residual stress of thin-walled parts in laser direct forming,” *Int J Adv Manuf Technol*, vol. 79, no. 1-4, pp. 81–88, 2015.
[24] J. J. Janosch, *IIW Round Robin protocol for residual stress and distortion prediction, Phase II (Proposal Rev. 1), IIW Doc. X/XV-RSDP-59-00*, 2000.
[25] K. Salonitis, L. D’Alvise, B. Schoinochoritis, D. Chantzis, “Additive manufacturing and post-processing simulation: Laser cladding followed by high speed machining,” *Int J Adv Manuf Technol*, vol. 85, no. 9-12, pp. 2401–2411, 2016.
[26] M. Gouge and P. Michaleris, “An Introduction to Additive Manufacturing Processes and Their Modeling Challenges,” in *Thermo-Mechanical Modeling of Additive Manufacturing*: Elsevier, 2018, pp. 3–18.
[27] M. Alimardani, E. Toyserkani, J. P. Huissoon, “A 3D dynamic numerical approach for temperature and thermal stress distributions in multilayer laser solid freeform fabrication process,” *Optics and Lasers in Engineering*, vol. 45, no. 12, pp. 1115–1130, 2007.